Arranging Ellipsoidal Particles in Three-Dimensional User-Specified Orientations with Ultrasound-Directed Self-Assembly

M. Prisbrey,[1] F. Guevara Vasquez,[2] and B. Raeymaekers[1,*]

[1] *Department of Mechanical Engineering, University of Utah, Salt Lake City, Utah 84112, USA*

[2] *Department of Mathematics, University of Utah, Salt Lake City, Utah 84112, USA*

(Received 28 March 2020; revised 22 May 2020; accepted 6 July 2020; published 11 August 2020)

Ultrasound-directed self-assembly (DSA) enables particles to be arranged into user-specified patterns, which finds application in a myriad of engineering applications. However, using ultrasound DSA with nonspherical particles requires the ability to explicitly control their orientation. We theoretically derive a method to determine the operating parameters (amplitude and phase) of any arrangement of ultrasound transducers required to explicitly align ellipsoidal particles in any three-dimensional user-specified orientation. This method locally minimizes the acoustic radiation potential at user-specified locations and optimizes the curvature of the acoustic radiation potential to direct ellipsoidal particles into user-specified orientations. We show experimental validation using a single ellipsoidal expanded polystyrene particle in air and quantify the difference between the user-specified and experimentally obtained orientations. This work finds application in using ultrasound DSA in industrial processes and as a manufacturing method for engineered materials.

DOI: 10.1103/PhysRevApplied.14.024026

I. INTRODUCTION

Directed self-assembly (DSA) is the process by which discrete components organize into patterns due to interactions between themselves and their environment, driven by internal or external forces [1]. DSA techniques enable the noninvasive manipulation of particles in a controlled fashion and, thus, are of interest to a myriad of engineering applications, including cell-cell interaction studies [2], biomedical devices [3], microfluidic devices [4], and for manufacturing engineered materials [5–8]. DSA is typically categorized into template [9,10], template-free [11], and external field-directed techniques [12–14]. Template DSA techniques require the mechanical [15] or chemical [16] modification of a substrate to create attraction sites that prompt selective particle deposition. Template-free DSA techniques employ chemically functionalized capping molecules that encapsulate particles and selectively interact with each other and the environment to organize the particles into patterns [17,18]. The complex fabrication methods required for template DSA typically limit dimensional scalability, whereas the finite selection of capping molecules restricts the types of patterns that template-free DSA techniques can organize. Alternatively, external-field-directed techniques employ a set of tunable transducers to generate electric [19], magnetic [20], and/or ultrasound [21–24] fields to noninvasively manipulate particles dispersed in a fluid into user-specified patterns. Tuning the operating parameters and spatial arrangement of the transducers allows the external field to be altered and, thus, the location where particles assemble. Magnetic and electric field DSA requires ferromagnetic and electrically conductive particles, respectively, and typically demand high-strength fields to manipulate particles into their desired location [25,26]. In contrast, ultrasound DSA relies on the convergence of the acoustic radiation force associated with an ultrasound wave field, which creates "acoustic traps" that capture and control the location of particles of any material type [27] and shape [28]. Furthermore, low attenuation of ultrasound waves in low-viscosity (bulk and shear) fluids [29], such as water [30], air [31–33], and photopolymer resin [8], facilitates dimensional scalability over macroscale areas and volumes. Also, the low-strength ultrasound wave field needed to perform ultrasound DSA renders it suitable for noninvasively manipulating fragile materials without causing damage, e.g., to manipulate biological materials [34,35].

Employing ultrasound DSA requires knowing the relationship between the ultrasound transducer operating parameters (amplitude and phase), their spatial arrangement, the corresponding ultrasound wave field, and the resulting pattern of particles. This relationship requires solving either the "forward" or "inverse" ultrasound DSA problem. The forward problem determines the pattern of particles that results from user-specified ultrasound transducer operating parameters, whereas the inverse problem

*bart.raeymaekers@utah.edu

computes the ultrasound transducer operating parameters required to assemble a user-specified pattern of particles. Conceptually, solving the inverse problem requires tuning the ultrasound transducer operating parameters to create an "acoustic trap" at user-specified locations where particles will accumulate. To accomplish this, the acoustic radiation force and potential associated with the standing ultrasound wave field must be zero and locally minimum, respectively, at user-specified locations where particles will accumulate [27].

Researchers have solved the inverse ultrasound DSA problem using an indirect approach by creating a database of solutions to the forward ultrasound DSA problem [36, 37], which does not provide a general solution to the inverse problem. The literature also documents different direct solution methodologies to the inverse ultrasound DSA problem, which enable the organization of two- (2D) [38–42] and three-dimensional (3D) [31,43] user-specified patterns of spherical particles. In addition to static patterns, few publications also demonstrate the assembly of dynamic patterns, in which spherical particles follow a user-specified trajectory [44,45]. However, existing solutions to the inverse problem neglect the orientation of the acoustic traps and, thus, only apply to organizing spherical particles because they are axisymmetric. This limitation prevents using ultrasound DSA with nonspherical particles, which is relevant to, for instance, manufacturing engineered composite materials with discontinuous aligned fibers. A few researchers have manipulated the orientation of ellipsoidal particles by modulating the amplitude of two orthogonal standing ultrasound waves [46] and by selectively energizing a subset of eight ultrasound transducers arranged as an octagon [47]. However, these methods rely on solving the forward ultrasound DSA problem in two dimensions and, thus, do not allow explicitly specifying a user-specified orientation and location of the particles, which is essential to using ultrasound DSA as e.g., a materials' manufacturing method. Furthermore, no demonstration exists in three dimensions. Marzo *et al.* derived a solution to the inverse ultrasound DSA problem for a single ellipsoidal particle by computing the ultrasound transducer operating parameters that maximize the Laplacian of the acoustic radiation potential with empirically derived weight functions, thereby implicitly controlling the orientation of a single disk-shaped particle in two dimensions [45]. Prisbrey and Raeymaekers computed the ultrasound transducer operating parameters required to maximize the curvature of the acoustic radiation potential associated with a 2D standing ultrasound wave field in any user-specified orientation and showed explicit control of the 2D orientation and position of multiple high-aspect-ratio particles (carbon microfibers) [48].

However, no theoretical understanding or experimental demonstration of using ultrasound DSA to explicitly control the orientation and location of nonspherical particles in three dimensions exists. Hence, the objective of this paper is to show the theoretical derivation of a direct solution method for the inverse ultrasound DSA problem to create 3D user-specified patterns of ellipsoidal particles with explicit user-specified orientation and location in three dimensions, for any arrangement and number of ultrasound transducers. We then show experimental validation of the theoretical method with a single ellipsoidal expanded polystyrene particle.

II. THEORETICAL DERIVATION

We follow a three-step procedure to create a pattern of ellipsoidal particles in three dimensions with explicit user-specified location and orientation. First, we compute the ultrasound (pressure) wave field resulting from any spatial arrangement of N_t ultrasound transducers as a function of their operating parameters. Second, we use Gor'kov's acoustic radiation force theory to compute the acoustic radiation force associated with the ultrasound wave field that acts on the ellipsoidal particles by treating a particle as a rigid bead chain of spherical particles, and we determine the resulting pattern of particles [27]. Third, we compute the ultrasound transducer operating parameters required to assemble any 3D pattern of ellipsoidal particles with explicit user-specified location and orientation by solving a constrained optimization problem. The objective function of the optimization problem simultaneously minimizes the acoustic radiation potential, U, to create acoustic traps at user-specified locations and optimizes the products of projections of its Hessian matrix in multiple directions to control the orientation of the acoustic traps, as a function of the ultrasound transducer operating parameters. Projecting the Hessian of U determines its curvature in that direction. Thus, we optimize the curvature of the acoustic radiation potential at each user-specified location in multiple directions, to ensure that the resulting acoustic radiation force is simultaneously small in the user-specified orientation and large in multiple directions orthogonal to the user-specified orientation. As a result, the acoustic traps at the user-specified locations are elongated in that direction and do not apply torque to ellipsoidal particles when their major axes align.

Figure 1 shows a Cartesian coordinate system (x,y,z) with origin $\mathbf{o}$ at the center of a ring structure with N_t evenly spaced ultrasound transducers, which create an ultrasound wave field with angular frequency $\omega_0 = 2\pi f_0$, where f_0 is the center frequency of the ultrasound transducers. The inset image in Fig. 1 identifies spatial parameters to describe the pressure originating from the jth ultrasound transducer at any discrete domain point $\mathbf{x}_l$ (red dots) in the 3D domain D. D contains a fluid medium with density ρ_0 and sound wave propagation speed c_0. The pressure wave field $\mathbf{P}$ at any point $\mathbf{x}_l$ is the summation of pressure waves emitted by all N_t ultrasound transducers with operating

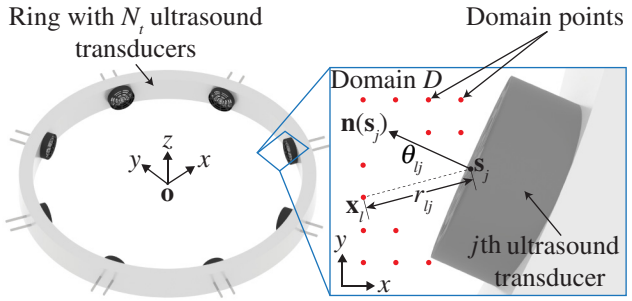

FIG. 1. Ring structure with N_t ultrasound transducers. Inset image identifies the spatial parameters to describe the ultrasound wave field at any domain point $\mathbf{x}_l$ (red dots), resulting from the j th ultrasound transducer with center at $\mathbf{s}_j$ (black dot) and normal direction $\mathbf{n}(\mathbf{s}_j)$.

parameters $\mathbf{v}$, which is computed in matrix form as

$$\mathbf{P} = \mathbf{B}\mathbf{v}. \tag{1}$$

Here,

$$\mathbf{v}^{\mathrm{T}} = (A_1 e^{i\alpha_1}, \ldots, A_j e^{i\alpha_j}, \ldots, A_{N_t} e^{i\alpha_{N_t}}), \tag{2}$$

and A_j and α_j are the amplitude and phase of the j th ultrasound transducer (with $j = 1 \ldots N_t$), respectively. $i = (-1)^{1/2}$. Matrix $\mathbf{B}$ relates the ultrasound transducer operating parameters $\mathbf{v}$ to the pressure wave field $\mathbf{P}$. Each element, p_{lj}, of $\mathbf{B}$ represents the pressure with no phase delay or amplitude modulation at the lth domain point $\mathbf{x}_l$ emitted from the j th ultrasound transducer [49], i.e.,

$$p_{lj} = 2P_0 \frac{J_1(k_0 a \sin(\theta_{lj}))}{k_0 a \sin(\theta_{lj})} \frac{e^{ik_0 r_{lj}}}{r_{lj}}. \tag{3}$$

Hence, the j th element of $\mathbf{v}$ scales and delays the pressure wave emitted from the j th ultrasound transducer with respect to domain point $\mathbf{x}_l$. We note that Eq. (3) assumes a circular piston source with radius a, and the 3D Euclidean distance r_{lj} between the lth domain point $\mathbf{x}_l$ and the j th ultrasound transducer center point $\mathbf{s}_j$ satisfies the far-field Fraunhofer limit, i.e., $r_{lj} >> a$ [49]. P_0 is an ultrasound transducer property [pressure amplitude in Pa per volt peak-to-peak (V_{PP}) square excitation signal at a distance from the ultrasound transducer] that relates the emitted pressure amplitude to the voltage signal amplitude driving the j th ultrasound transducer. J_1 is the first-order Bessel function of the first kind, $k_0 = 2\pi/\lambda_0$ is the wave number, $\lambda_0 = c_0/f_0$ is the wavelength of the ultrasound wave field, and θ_{lj} is the angle between the lth domain point $\mathbf{x}_l$ and the j th ultrasound transducer normal vector $\mathbf{n}(\mathbf{s}_j)$.

Gor'kov's acoustic radiation force theory describes the acoustic radiation potential at the lth domain point $\mathbf{x}_l$ as $U_l = \mathbf{v}^{\mathrm{T}} \mathrm{Q}_l \mathbf{v}$ and [27,50]

$$\mathbf{Q}_l = 2\Phi_1(\mathbf{B}_l \mathbf{B}_l^H) - 2\Phi_2[(\nabla \mathbf{B}_l)(\nabla \mathbf{B}_l)^H]. \tag{4}$$

With acoustic contrast factors

$$\Phi_1 = \frac{\pi r_p^3}{3}\left(\frac{1}{c_0^2 \rho_0} - \frac{1}{c_p^2 \rho_p}\right), \tag{5}$$

$$\Phi_2 = \pi r_p^3 \left[\frac{\rho_p - \rho_0}{\omega_0 \rho_0 (\rho_0 + 2\rho_p)}\right]. \tag{6}$$

The term $\mathbf{B}_l$ in Eq. (4) is the lth row of $\mathbf{B}$, and the superscript H represents the complex conjugate transpose. The acoustic radiation force $\mathbf{F}_l = -\nabla U_l$ at the lth domain point $\mathbf{x}_l$ acts on each spherical particle (of the bead chain that approximates the ellipsoidal particle) with radius $r_p << \lambda_0$, density ρ_p, and sound propagation speed c_p in domain D. Thus, Gor'kov's acoustic radiation force theory relates the ultrasound wave field to the locations of acoustic traps where particles will accumulate [27], which are defined as the stable fixed locations $\mathbf{x}_s \in D$, where the magnitude of the acoustic radiation force $|\mathbf{F}_l| = 0$ and points toward $\mathbf{x}_s$ in the surrounding region.

We define the orientation of an ellipsoidal particle in an acoustic trap at $\mathbf{x}_s$ as the direction of a unit vector $\mathbf{e}_k$ that coincides with the major axis of the ellipsoidal particle. Figure 2 shows two Cartesian coordinate systems in D, showing orthonormal basis vectors $\{\mathbf{e}_x, \mathbf{e}_y, \mathbf{e}_z\}$ with origin $\mathbf{o}$ and orthonormal basis vectors $\{\mathbf{e}_i, \mathbf{e}_j, \mathbf{e}_k\}$ with origin $\mathbf{x}_s$; $\mathbf{e}_z$ represents the direction of gravity. We determine the

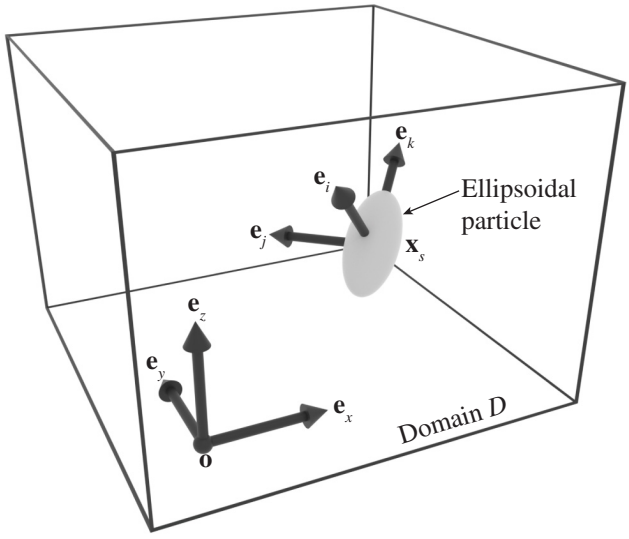

FIG. 2. Domain D with Cartesian coordinate systems $\{\mathbf{e}_x, \mathbf{e}_y, \mathbf{e}_z\}$ with origin $\mathbf{o}$ and $\{\mathbf{e}_i, \mathbf{e}_j, \mathbf{e}_k\}$ with origin $\mathbf{x}_s$ that contain an ellipsoidal particle.

orientation $\mathbf{e}_k$ of an acoustic trap at $\mathbf{x}_s$ via the relationship between the curvature $\kappa(\mathbf{x}_s,\mathbf{e}_n)$ of the acoustic radiation potential U at $\mathbf{x}_s$ in each of the three directions $\mathbf{e}_n = \mathbf{e}_i$, $\mathbf{e}_j$, and $\mathbf{e}_k$. Note that, $\mathbf{e}_n$ is a unit vector with origin $\mathbf{x}_s$ that defines the direction in which we determine the curvature of the acoustic radiation potential U.

We compute the curvature of the acoustic radiation potential U_l at any domain point $\mathbf{x}_l$ in the direction of $\mathbf{e}_n$ as

$$\kappa(\mathbf{x}_l, \mathbf{e}_n) = \mathbf{v}^H \mathbf{K}_l^{\mathbf{e}_n} \mathbf{v}, \tag{7}$$

where $\mathbf{K}_l^{\mathbf{e}_n} = {\mathbf{e}_n}^T \mathbf{H}_l \mathbf{e}_n$ is a projection of the Hessian matrix of the acoustic radiation potential $\mathbf{H}_l$ in the direction of $\mathbf{e}_n$. The orientation $\mathbf{e}_k$ of an acoustic trap $\mathbf{x}_s$ is the direction $\mathbf{e}_n$, for which the curvature of the acoustic radiation potential $\kappa(\mathbf{x}_s,\mathbf{e}_n) = 0$, with the additional requirement that the other two curvatures associated with the particle coordinate system $\kappa(\mathbf{x}_s,\mathbf{e}_i) \approx \kappa(\mathbf{x}_s,\mathbf{e}_j) > 0$ to ensure that the particle does not rotate in the $\mathbf{e}_k$-$\mathbf{e}_j$ or $\mathbf{e}_k$-$\mathbf{e}_i$ planes. $\mathbf{H}_l$ is computed as

$$\mathbf{H}_l = \begin{pmatrix} \frac{\partial^2 \mathbf{Q}_l}{\partial x^2} & \frac{\partial^2 \mathbf{Q}_l}{\partial x \partial y} & \frac{\partial^2 \mathbf{Q}_l}{\partial x \partial z} \\ \frac{\partial^2 \mathbf{Q}_l}{\partial y \partial x} & \frac{\partial^2 \mathbf{Q}_l}{\partial y^2} & \frac{\partial^2 \mathbf{Q}_l}{\partial y \partial z} \\ \frac{\partial^2 \mathbf{Q}_l}{\partial z \partial x} & \frac{\partial^2 \mathbf{Q}_l}{\partial z \partial y} & \frac{\partial^2 \mathbf{Q}_l}{\partial z^2} \end{pmatrix}. \tag{8}$$

X_d and E_d are lists in which each element represents a 3D user-specified location $\mathbf{x}_d$ and orientation $\mathbf{e}_d$ of an ellipsoidal particle in D, respectively. Hence, to assemble ellipsoidal particles at all $\mathbf{x}_d \in X_d$ with the corresponding curvature $\mathbf{e}_d \in E_d$, the curvature $\kappa(\mathbf{x}_d,\mathbf{e}_d) = 0$ and the curvature in two mutually orthogonal directions $\kappa(\mathbf{x}_d,\mathbf{e}_i)$ and $\kappa(\mathbf{x}_d,\mathbf{e}_j)$ must be approximately equal and positive, i.e., $\kappa(\mathbf{x}_d,\mathbf{e}_i) \approx \kappa(\mathbf{x}_d,\mathbf{e}_j) > 0$ for all elements of X_d and E_d. Additionally, the acoustic radiation potential U must be locally minimum at all $\mathbf{x}_d \in X_d$. We represent an ellipsoidal particle as a rigid bead chain of spherical particles, similar to our previous work [48], and we account for the length of an ellipsoidal particle by including the $\{x, y, z\}$ coordinates of each bead on the bead chain that represents each ellipsoidal particle in X_d. Thus, we describe patterns of multiple ellipsoidal particles by including the coordinates of their respective bead chains in X_d. To compute the ultrasound transducer operating parameters required to assemble patterns of ellipsoidal particles with explicit user-specified orientations and positions, we formulate an objective function that simultaneously maximizes the product $\kappa(\mathbf{x}_d,\mathbf{e}_i)\kappa(\mathbf{x}_d,\mathbf{e}_j)$ to ensure they are approximately equal, minimizes $\kappa(\mathbf{x}_d,\mathbf{e}_d)^2$ to ensure that the curvature in the user-specified orientation $\mathbf{e}_d$ is zero, and minimizes the acoustic radiation potential U to ensure an acoustic trap exists for all points $\mathbf{x}_d \in X_d$. To obtain a single objective function and optimize for all user-specified locations $\mathbf{x}_d \in X_d$ and corresponding orientations $\mathbf{e}_d \in E_d$ simultaneously, we relax the requirement of local maximality by maximizing the sum of the curvature for all points $\mathbf{x}_d \in X_d$ and the corresponding orientation $\mathbf{e}_d \in E_d$, which we express in quadratic form as a function of the ultrasound transducer operating parameters $\mathbf{v}$, i.e.,

$$\kappa_\Sigma(\mathbf{x}_d, \mathbf{e}_n) = \mathbf{v}^H \mathbf{K}_\Sigma^{\mathbf{e}_n} \mathbf{v}. \tag{9}$$

Here, $\mathbf{K}_\Sigma{}^{\mathbf{e}_n}$ is the summation of matrices $\mathbf{K}_l{}^{\mathbf{e}_n}$ for all points $\mathbf{x}_d \in X_d$. Similar to Greenhall *et al.* [38], we constrain the amplitude of the ultrasound transducers $|\mathbf{v}| = \beta$ to reflect their finite input power, where β is a real scalar value that represents the maximum harmonic velocity of the ultrasound transducer surface. Thus, we formulate the constrained quartic objective function as

$$\begin{aligned} \max_{\mathbf{v}} f(\mathbf{v}) = {} & \kappa_\Sigma(\mathbf{x}_d, \mathbf{e}_i)\kappa_\Sigma(\mathbf{x}_d, \mathbf{e}_j) - \kappa_\Sigma(\mathbf{x}_d, \mathbf{e}_d)^2 \\ & + \varsigma \kappa_\Sigma(\mathbf{x}_d, \mathbf{e}_z)^2 - \delta \mathbf{v}^H \mathbf{Q}_\Sigma \mathbf{v}, \\ & \text{subject to } |\mathbf{v}| = \beta. \end{aligned} \tag{10}$$

Matrix $\mathbf{Q}_\Sigma$ is the summation of matrices $\mathbf{Q}_l$ for all $\mathbf{x}_d \in X_d$. Maximizing Eq. (10) determines the optimal ultrasound transducer operating parameters (amplitude and phase) $\mathbf{v}^*$ required to assemble ellipsoidal particles with explicitly defined 3D user-specified locations and orientations. Note that, $\varsigma \kappa_\Sigma(\mathbf{x}_d, \mathbf{e}_z)^2$ compensates for the gravitational force acting on the particle by maximizing the squared curvature of U in direction $\mathbf{e}_z$, and ensures that the acoustic radiation force is sufficiently large to levitate a particle. ς is a calibration constant that accounts for the particle properties. If this term is too small, the acoustic radiation force may be too small to levitate a particle. Conversely, if it is too large, the term will dominate the objective function, resulting in an ultrasound wave field that may cause the particle to rotate in the plane orthogonal to the direction of gravity. Additionally, $-\delta \mathbf{v}^H \mathbf{Q}_\Sigma \mathbf{v}$ ensures that the resulting acoustic radiation potential U is locally minimum at the user-specified locations $\mathbf{x}_d \in X_d$. This is important when maximizing $\kappa_\Sigma(\mathbf{x}_d,\mathbf{e}_i)\kappa_\Sigma(\mathbf{x}_d,\mathbf{e}_j)$ because it enables the resulting curvatures $\kappa_\Sigma(\mathbf{x}_d,\mathbf{e}_i) > 0$ and $\kappa_\Sigma(\mathbf{x}_d,\mathbf{e}_j) > 0$. Otherwise it is possible to maximize $\kappa_\Sigma(\mathbf{x}_d,\mathbf{e}_i)\kappa_\Sigma(\mathbf{x}_d,\mathbf{e}_j)$ with $\kappa_\Sigma(\mathbf{x}_d,\mathbf{e}_i) < 0$ and $\kappa_\Sigma(\mathbf{x}_d,\mathbf{e}_j) < 0$, which creates a local maximum rather than a minimum in U at $\mathbf{x}_d$ and, thus, would not be a stable fixed point ("acoustic trap"). δ is a calibration constant to ensure $\kappa_\Sigma(\mathbf{x}_d,\mathbf{e}_i) > 0$ and $\kappa_\Sigma(\mathbf{x}_d,\mathbf{e}_j) > 0$. If this term is too small, the resulting acoustic radiation potential may not create acoustic traps at the user-specified locations. Conversely, if it is too large, it will dominate the other terms, effectively reducing Eq. (10) to $\max_{\mathbf{v}} -\mathbf{v}^H \mathbf{Q}_\Sigma \mathbf{v}$. We have solved the latter optimization problem previously [38,43,44], to create user-specified patterns of spherical particles, but it does not provide explicit control over

the orientation of ellipsoidal particles. We design an optimization algorithm to maximize Eq. (10) by successive eigendecompositions of matrices of the same size as $\mathbf{Q}_\Sigma$. The algorithm guarantees the generation of a sequence of iterates that converge in objective function values [51].

III. METHODS AND MATERIALS

We experimentally demonstrate the theoretical solution method to the inverse ultrasound DSA problem for a single ellipsoidal particle. The process to manipulate a single ellipsoidal particle into an explicitly defined orientation is as follows. We first define a user-specified orientation $\mathbf{e}_d$ and location $\mathbf{x}_d$ such that the bead (of the bead chain that approximates the ellipsoidal particle) at the center of the particle coincides with the center ($\mathbf{x}_d = \mathbf{o}$) of a fluid reservoir with a specific shape and spatial arrangement of N_t ultrasound transducers. We then maximize Eq. (10) to compute the optimal ultrasound transducer operating parameters $\mathbf{v}^*$ required to orient the ellipsoidal particle in the user-specified orientation $\mathbf{e}_d$ with its center at $\mathbf{x}_d = \mathbf{o}$, accounting for the reservoir shape and spatial arrangement of transducers. Finally, we experimentally validate the theoretical model by applying the resulting optimal ultrasound transducer operating parameters $\mathbf{v}^*$ to an experimental setup with an identical fluid reservoir and spatial arrangement of N_t ultrasound transducers and by measuring the experimentally obtained orientation of the ellipsoidal particle compared with the user-specified orientation.

Figure 3 schematically shows the experimental setup with an ellipsoidal particle at its center (not to scale). We use an EPS particle ($c_p = 900$ m/s, $\rho_p = 25$ kg/m^3) in air

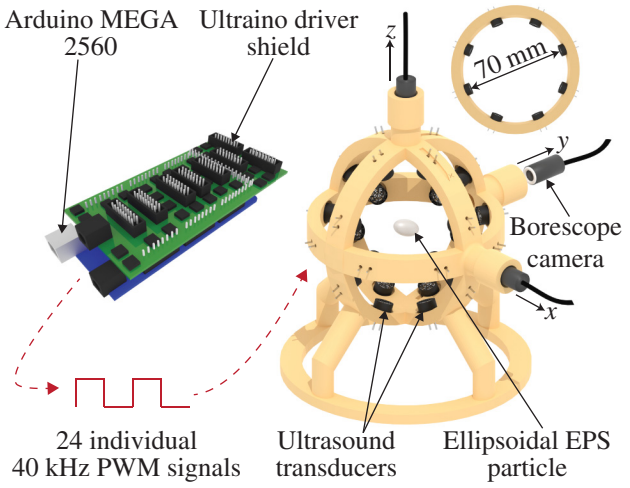

FIG. 3. Schematic of the experimental setup, comprising three rings with eight ultrasound transducers each, showing an ellipsoidal expanded polystyrene (EPS) particle at its center. Ultrasound transducers are driven by 40 kHz pulse-width-modulated (PWM) signals.

($c_0 = 346$ m/s, $\rho_0 = 1.18$ kg/m^3). The average lengths of the major and minor axes of the EPS particles are 4.2 and 2.1 mm, respectively. The setup comprises three identical orthogonal rings with diameter 70 mm that define a spherical reservoir, each with eight uniformly distributed ultrasound transducers (type Murata MA40S4S) of radius $a = 4.5$ mm [see Eq. (3)] that have a directivity of 80° and a center frequency $f_0 = 40$ kHz. We design the rings with a diameter of 70 mm, about $8\lambda_0$ ($\lambda_0 = 8.65$ mm), to ensure that the acoustic trap at $\mathbf{x}_d = \mathbf{o}$ is in the far-field region. We use an Arduino Mega 2560 board with an ULTRAINO driver shield [52] to drive each ultrasound transducer with an independently controlled PWM signal. The ULTRAINO driver shield amplifies 5 V PWM signals generated with the Arduino Mega 2560 board to a maximum of 18 V via MOSFET amplifying circuits. Altering the PWM duty cycle and adding a delay enable the independent control of the amplitude and phase of each ultrasound transducer. Furthermore, the experimental setup is fitted with three borescope cameras that view along the negative x, y, and z axes to create image projections of the EPS particles on three orthogonal planes that intersect at the center of the rings. We manufacture the structure of the experimental setup using fused deposition modeling with polylactic acid plastic. Figure 3 also shows an inset image of a single ring to illustrate its dimensions and placement of the ultrasound transducers.

Figure 4(a) shows a simplified schematic of the experimental setup, with the borescope cameras and support structure removed for clarity, and with an ellipsoidal EPS particle (not to scale) at its center. The inset image depicts intersecting x-y, x-z, and y-z view planes, as viewed from the perspective of the borescope cameras, with the EPS particle at its center. Figure 4(b) shows the projections of the EPS particle on each view plane, indicating the angles θ_m and φ_m, which represent the rotation of the EPS particle about the z axis and about an axis in the x-y plane, respectively. We measure θ_m and φ_m based on the major axis of the EPS particle [light blue arrows in Fig. 4(b)]. We compute the major axis using principal-component analysis on binarized versions of the borescope images. We then compute the orientation $\mathbf{e}_m$ of the EPS particle in the experiment as

$$\mathbf{e}_m = \begin{bmatrix} \cos(\theta_m)\cos(\varphi_m) \\ \sin(\theta_m)\cos(\varphi_m) \\ -\sin(\varphi_m) \end{bmatrix}. \tag{11}$$

We note that the user-specified orientation $\mathbf{e}_d$ can also be expressed via user-specified angles θ_d and φ_d. We define the orientation error as the angle γ_e between the user-specified orientation $\mathbf{e}_d$ and the experimentally determined orientation of the EPS particle $\mathbf{e}_m$,

$$\gamma_e = \arccos(\mathbf{e}_d \cdot \mathbf{e}_m). \tag{12}$$

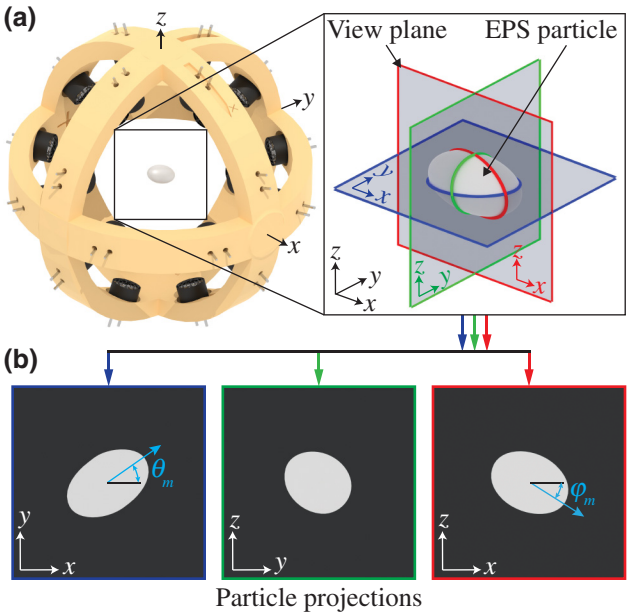

FIG. 4. (a) Simplified experimental setup schematic with an ellipsoidal EPS particle in the center. Inset shows orthogonal view planes that intersect the particle to create projections. (b) EPS particle projections on the x-y, x-z, and y-z view planes.

IV. RESULTS AND DISCUSSION

We experimentally demonstrate explicit control of the 3D location and orientation of a single ellipsoidal EPS particle for several user-specified angles θ_d with $\varphi_d = 0$ (Fig. 5) and for several user-specified angles θ_d with $\varphi_d = 10$, 20, and 30° (Fig. 6). For all experiments, the user-specified location is at the center of the experimental setup ($\mathbf{x}_d = \mathbf{0}$). Figures 5(a) and 6(a) show experimental results (orthogonal projections of the EPS particle) with the user-specified angles θ_d and φ_d indicated in orange. Additionally, Figs. 5(b) and 6(b) show the orientation error γ_e as a function of the user-specified angles θ_d and φ_d.

Figure 5(a) shows orthogonal projections of an ellipsoidal EPS particle (white) oriented at user-specified angles $\theta_d = 0$, 45, and 135° with $\varphi_d = 0°$. Each row pertains to a single experiment. The middle column shows projections of the EPS particle on the x-y plane and the right column shows projections on the x-z or y-z planes. We observe good qualitative agreement between the user-specified orientations and experimentally measured orientation of the EPS particle. Figure 5(b) shows the orientation error γ_e as a function of the user-specified orientation angle θ_d with $\varphi_d = 0°$. We observe a maximum orientation error of 22.8° for $\theta_d = 70°$ and minimum orientation error of 2.8° for $\theta_d = 20°$. Prisbrey and Raeymaekers have previously used ultrasound DSA to assemble 2D patterns of high-aspect-ratio carbon microfibers with user-specified orientation in water. They computed the optimal operating parameters of $N_t = 16$ ultrasound transducers,

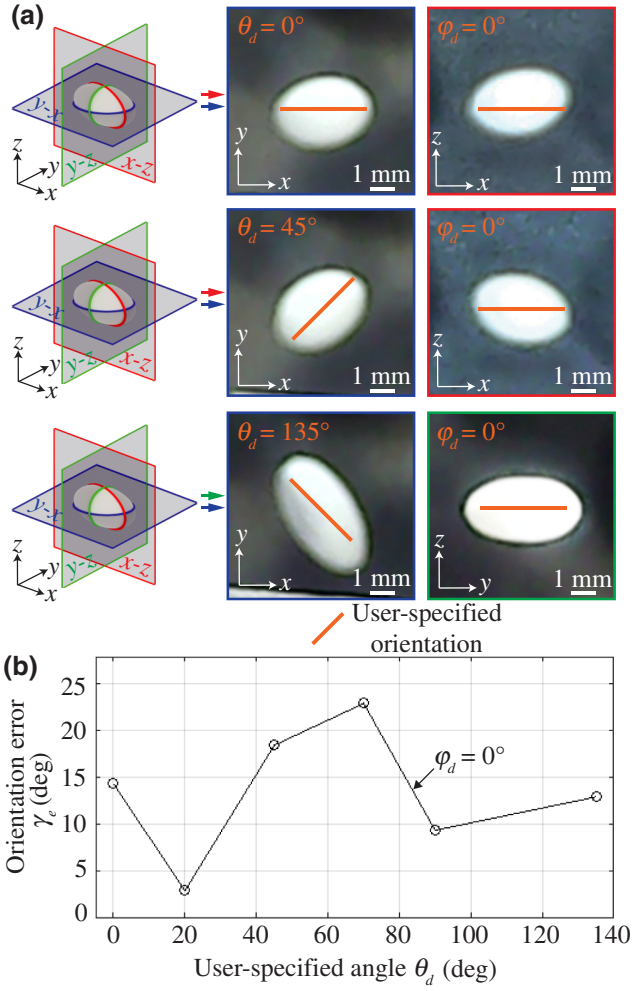

FIG. 5. (a) Experimentally obtained projections of ellipsoidal EPS particle projections for $\theta_d = 0$, 45, and 135° and $\varphi_d = 0°$. (b) Orientation error as a function of θ_d and $\varphi_d = 0°$.

arranged as a hexadecagon, by maximizing the curvature of the acoustic radiation potential in a user-specified orientation [48]. This method does not allow explicit control of the 3D user-specified orientations of high-aspect-ratio particles, but in the limiting case, where $\varphi_d = 0°$ and, thus, the high-aspect-ratio particle is oriented in two dimensions, the method presented here must yield similar experimental results to those obtained using the method presented in Ref. [48]. Indeed, Prisbrey and Raeymaekers report a similar, yet slightly smaller, orientation error in Ref. [48]. The 2D experiments [48] do not require simultaneously orienting and levitating the high-aspect-ratio particles because they are performed in water, which provides buoyancy forces that easily levitate the carbon microfibers. Therefore, the 2D method only uses the ultrasound transducers to orient the high-aspect-ratio particles. However, in the 3D method derived in this paper, a subset of ultrasound transducers must maximize the curvature of the acoustic radiation potential in the $\mathbf{e}_z$ direction [see Eq. (10)], to

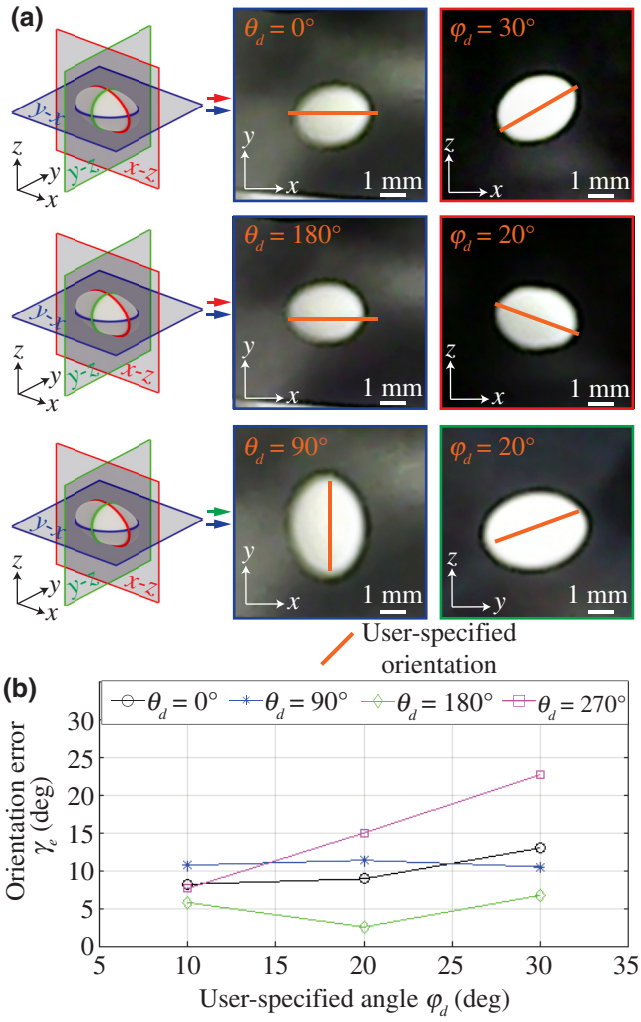

FIG. 6. (a) Experimentally obtained projections of an ellipsoidal EPS particle for $\theta_d = 0$, 90, and 180° and $\varphi_d = 20$ and 30°. (b) Orientation error as a function of θ_d and φ_d.

create a component of the acoustic radiation force that levitates the ellipsoidal EPS particle. Thus, this decreases the number of ultrasound transducers available to orient the ellipsoidal particle in the x-y plane, which affects the accuracy. Additionally, the objective function derived in this paper maximizes the curvature of the acoustic radiation potential in $\mathbf{e}_i$ and $\mathbf{e}_j$ orthogonal to $\mathbf{e}_d$ and, thus, the component of the acoustic radiation forces in directions between $\mathbf{e}_i$ and $\mathbf{e}_j$ may be small, which would allow the particle to "slip" and/or rotate in between the $\mathbf{e}_d\mathbf{e}_i$ and $\mathbf{e}_d\mathbf{e}_i$ planes. In the 2D method [48], maximizing the curvature of the acoustic radiation potential in a single direction precludes this problem. In three dimensions, solving this problem requires maximization of the curvature of the acoustic radiation potential in many or even an infinite number of directions orthogonal to $\mathbf{e}_d$. However, this could further relax the requirement of local maximality of the objective function and increase the error.

Figure 6(a) shows projections of an ellipsoidal EPS particle (white) oriented at user-specified angles $\theta_d = 0$, 90, and 180° with $\varphi_d = 20$ and 30°. Each row pertains to a single experiment. The middle column shows projections of the EPS particle on the x-y plane and the right column shows projections on the x-z or y-z planes. We observe good qualitative agreement between the user-specified orientations and experimentally measured orientation of the ellipsoidal EPS particle. Figure 6(b) shows the orientation error γ_e as a function of the user-specified angles θ_d and φ_d, which is similar to the orientation error of Fig. 5(b) for a user-specified orientation in the x-y plane. The orientation error tends to increase when $\varphi_d > 20°$, which results from increasing the curvature of the acoustic radiation potential in the z direction to levitate the ellipsoidal EPS particle, even when its projection on the x-y plane decreases. When the ellipsoidal particle rotates out of the x-y plane, the user-specified orientation $\mathbf{e}_d$ tends toward the z axis ($\mathbf{e}_z$), which results in competing terms in the objective function. Specifically, the term that minimizes the squared curvature of the acoustic radiation potential in the user-specified orientation $\mathbf{e}_d$ and the gravity compensation term [see Eq. (10)] combine when $\mathbf{e}_d$ coincides with the z axis. Decreasing the influence of the gravity compensation term in the objective function, by either decreasing the weight of the particles and/or increasing the total acoustic radiation force on the particle by adding ultrasound transducers to the setup, solves this problem. Additionally, a study by Cox *et al.* indicates that decreasing the dependence on the gravity compensation term may be possible by rapidly alternating between multiple acoustic traps to create a "composite" acoustic trap, where one acoustic trap provides large acoustic radiation forces in the direction of gravity, and the second acoustic trap works to orient the elongated particles [53]. This, however, increases the complexity of controlling the experimental setup, due to the need to rapidly alter the signals driving the ultrasound transducers.

The orientation error in all experiments also results from the following. We treat the ellipsoidal particles as a rigid bead chain of spheres, for which Gor'kov's acoustic radiation force theory is not strictly valid. Furthermore, the aspect ratio of an ellipsoid is smaller than that of a bead chain. This, however, still enables accurate location and orientation of the ellipsoidal particles, as indicated by the small orientation error. Manufacturing errors in the experimental setup result in misalignment of the ultrasound transducers, which causes the theoretical and experimental spatial arrangement of the ultrasound transducers to be different. The ULTRAINO software has limited amplitude and phase resolution of $V_{PP}/10$ between 0 and 18 V_{PP} and $\pi/5$ radians, respectively, which are both accounted for in our simulation, yet, nevertheless, pose a limitation to the solution of the inverse ultrasound DSA problem. The objective function presented in Eq. (10) is relaxed both

because we sum over all points $\mathbf{x}_d \in X_d$ and because we include multiple terms, which may confound with each other, and result in acoustic traps that form nearby user-specified locations and/or in orientations that deviate from the user-specified orientations. Furthermore, deviations between the user-specified and experimentally obtained orientation result from scattering of the ultrasound wave field off nearby surfaces, which is not accounted for in the calculation of the acoustic pressure.

We levitate ellipsoidal EPS particles in air to experimentally demonstrate and visualize that the solution to the inverse ultrasound DSA problem derived in this work allows the orientation of high-aspect-ratio particles to be explicitly accounted for. However, we emphasize that this solution also translates to systems of varying size and shape, with different particle shapes and different fluid media. Thus, the solution to the inverse ultrasound DSA problem for aligning ellipsoid particles in 3D user-specified orientations apply to, e.g., employing ultrasound DSA as a processing method for engineered materials that derive their properties from a pattern of high- aspect ratio particles embedded in a matrix material.

We point out that it is possible to specify a pattern of ellipsoidal particles with a user-specified location and orientation that cannot be implemented because not all possible user-specified locations and orientations yield a solution that maximizes Eq. (10). Increasing the number of ultrasound transducers increases the possibility of maximizing Eq. (10) for many different user-specified locations and orientations. However, the relationship between the number of ultrasound transducers, their spatial arrangement, and achievable patterns of particles remains an open problem. Additionally, the formation of acoustic traps in locations that are not part of the user-specified pattern are an inevitable result of interference between ultrasound waves that generate the acoustic traps in user-specified locations. We note that the possibility of a particle vibrating within an acoustic trap is an inherent limitation of ultrasound DSA, which could lead to increased instability over time and cause the ellipsoidal particle to eject from the acoustic trap [54]. However, during the experiments in this work we do not observe increasing instability over time while the particle rests in the acoustic trap during imaging.

V. CONCLUSION

We theoretically derive and experimentally demonstrate a direct solution to the inverse ultrasound DSA problem that enables explicit control over the 3D location and orientation of an ellipsoidal particle. This solution method contrasts earlier solutions of the inverse ultrasound DSA problem limited to 3D user-specified patterns of spherical particles and 2D user-specified patterns of high-aspect-ratio particles. Maximizing the curvature of the acoustic radiation potential in two orthogonal directions, and orthogonal to the user-specified direction of the ellipsoidal particle, allows explicit control over its 3D orientation. Experimental measurements of the orientation of a single ellipsoidal EPS particle, relative to the user-specified orientation, reveal a slightly larger orientation error for the method that explicitly orients ellipsoidal particles in three dimensions, compared with the 2D method published earlier. This increased error results from the need to simultaneously levitate and orient the ellipsoidal particle in three dimensions, rather than just orient it in two dimensions. This work has implications for using ultrasound DSA as a manufacturing method for engineered materials that derive their properties from specifically oriented fibers embedded in a matrix material, including electrically conductive materials with embedded wiring, or for structurally reinforced composite materials, to only name a few.

ACKNOWLEDGMENTS

This research is supported by the Army Research Office under Contract No. W911NF-16-1-0457. The authors thank Dr. Asier Marzo for providing the ULTRAINO software and hardware construction process.

[1] M. Grzelczak, J. Vermant, E. M. Furst, and L. M. Liz-Marzán, Directed self-assembly of nanoparticles, ACS Nano **4**, 3591 (2010).
[2] M. Evander and J. Nilsson, Acoustofluidics 20: Applications in acoustic trapping, Lab Chip **12**, 4667 (2012).
[3] Y. Yamakoshi, Y. Koitabashi, N. Nakajima, and T. Miwa, Yeast cell trapping in ultrasonic wave field using ultrasonic contrast agent, Jpn. J. Appl. Phys. **45**, 4712 (2006).
[4] B. Jung, K. Fisher, K. D. Ness, K. A. Rose, and R. P. Mariella, Acoustic particle filter with adjustable effective pore size for automated sample preparation, Anal. Chem. **80**, 8447 (2008).
[5] J. N. Coleman, U. Khan, W. J. Blau, and Y. K. Gun'ko, Small but strong: A review of the mechanical properties of carbon nanotube-polymer composites, Carbon **44**, 1624 (2006).
[6] V. M. Shalaev, Optical negative-index metamaterials, Nat. Photonics **1**, 41 (2007).
[7] S. J. Corbitt, M. Francoeur, and B. Raeymaekers, Implementation of optical dielectric metamaterials: A review, J. Quant. Spectrosc. Radiat. Transf. **158**, 3 (2015).
[8] J. Greenhall and B. Raeymaekers, 3D printing macroscale engineered materials using ultrasound directed self-assembly and stereolithography, Adv. Mater. Technol. **2**, 170122 (2017).
[9] Z. Nie, A. Petukhova, and E. Kumacheva, Properties and emerging applications of self-assembled structures made from inorganic nanoparticles, Nat. Nanotechnol. **5**, 15 (2010).
[10] S. B. Darling, Directing the self-assembly of block copolymers, Prog. Polym. Sci. **32**, 1152 (2007).

[11] E. Dujardin, L.-B. Hsin, C. R. Chris Wang, and S. Mann, DNA-driven self-assembly of gold nanorods, Chem. Commun. **0**, 1264 (2001).

[12] K. D. Hermanson, S. O. Lumsdon, J. P. Williams, E. W. Kaler, and O. D. Velev, Dielectrophoretic assembly of electrically functional microwires from nanoparticle suspensions, Science **294**, 1082 (2001).

[13] J. H. E. Promislow and A. P. Gast, Magnetorheological fluid structure in a pulsed magnetic field, Langmuir **12**, 4095 (1996).

[14] B. Raeymaekers, C. Pantea, and D. N. Sinha, Dynamic behavior of microscale particles controlled by standing bulk acoustic waves, J. Appl. Phys. **109**, 014317 (2011).

[15] T. D. Clark, R. Ferrigno, J. Tien, K. E. Paul, and G. M. Whitesides, Template-Directed self-assembly of 10-μm-sized hexagonal plates, J. Am. Chem. Soc. **124**, 5419 (2002).

[16] Y. Pan, M. Gao, L. Huang, F. Liu, and H.-J. Gao, Directed self-assembly of monodispersed platinum nanoclusters on graphene moiré template, Appl. Phys. Lett. **95**, 093106 (2009).

[17] A. Sunna, A. Care, and P. L. Bergquist, *Peptides and Peptide-Based Biomaterials and Their Biomedical Applications* (Springer, Basil, Switzerland, 2017).

[18] M. Fialkowski, K. J. M. Bishop, R. Klajn, S. K. Smoukov, C. J. Campbell, and B. A. Grzybowski, Principles and implementations of dissipative (dynamic) self-assembly, J. Phys. Chem. B **110**, 2482 (2006).

[19] Q. Wang, J. Dai, W. Li, Z. Wei, and J. Jiang, The effects of CNT alignment on electrical conductivity and mechanical properties of SWNT/epoxy nanocomposites, Compos. Sci. Technol. **68**, 1644 (2008).

[20] S. K. Smoukov, S. Gangwal, M. Marquez, and O. D. Velev, Reconfigurable responsive structures assembled from magnetic janus particles, Soft Matter **5**, 1285 (2009).

[21] K. Niendorf and B. Raeymaekers, Quantifying macro- and microscale alignment of carbon microfibers in polymer-matrix composite materials fabricated using ultrasound directed self-assembly and 3D-printing, Compos. Part A Appl. Sci. Manuf. **129**, 105713 (2020).

[22] D. Baresch, J.-L. Thomas, and R. Marchiano, Observation of a Single-Beam Gradient Force Acoustical Trap for Elastic Particles: Acoustical Tweezers, Phys. Rev. Lett. **116**, 024301 (2016).

[23] D. Baresch, J.-L. Thomas, and R. Marchiano, Orbital Angular Momentum Transfer to Stably Trapped Elastic Particles in Acoustical Vortex Beams, Phys. Rev. Lett. **121**, 074301 (2018).

[24] J. Greenhall, F. Guevara Vasquez, and B. Raeymaekers, Dynamic behavior of microscale particles controlled by standing bulk acoustic waves, Appl. Phys. Lett. **105**, 144105 (2014).

[25] M. Fujiwara, E. Oki, M. Hamada, Y. Tanimoto, I. Mukouda, and Y. Shimomura, Magnetic orientation and magnetic properties of a single carbon nanotube, J. Phys. Chem. A **105**, 4383 (2001).

[26] P. V. Kamat, K. G. Thomas, S. Barazzouk, G. Girishkumar, K. Vinodgopal, and D. Meisel, Self-assembled linear bundles of single wall carbon nanotubes and their alignment and deposition as a film in a dc field, J. Am. Chem. Soc. **126**, 10757 (2004).

[27] L. P. Gor'kov, On the acoustic radiation pressure on spheres, Sov. Phys. Dokl. **6**, 773 (1962).

[28] R. R. Collino, T. R. Ray, R. C. Fleming, C. H. Sasaki, H. Haj-Hariri, and M. R. Begley, Acoustic field controlled patterning and assembly of anisotropic particles, Extreme Mech. Lett. **5**, 37 (2015).

[29] L. E. Kinsler, A. R. Frey, A. B. Coppens, and J. V. Sanders, *Fundamentals of Acoustics*, 4th ed (John Wiley, New York, 2000).

[30] C. R. P. Courtney, B. W. Drinkwater, C. E. M. Demore, S. Cochran, A. Grinenko, and P. D. Wilcox, Dexterous manipulation of microparticles using Bessel-function acoustic pressure fields, Appl. Phys. Lett. **102**, 123508 (2013).

[31] Y. Ochiai, T. Hoshi, and J. Rekimoto, Three-dimensional mid-air acoustic manipulation by ultrasonic phased arrays, PLoS One **9**, e102525 (2014).

[32] A. Marzo, A. Barnes, and B. W. Drinkwater, Tinylev: A multi-emitter single-axis acoustic levitator, Rev. Sci. Instrum. **88**, 085105 (2017).

[33] D. Foresti, M. Nabavi, M. Klingauf, A. Ferrari, and D. Poulikakos, Acoustophoretic contactless transport and handling of matter in air, PNAS **110**, 12549 (2013).

[34] R. H. Morris, E. R. Dye, D. Axford, M. I. Newton, J. H. Beale, and P. T. Docker, Non-contact inversal sample presentation for room temperature macromolecular crystallography using acoustic levitation, Sci. Rep. **9**, 12431 (2019).

[35] Z. Yang, K. L. H. Cole, Y. Qiu, I. M. L. Somorjai, P. Wijesinghe, J. Nylk, S. Cochran, G. C. Spalding, D. A. Lyons, and K. Dholakia, Light sheet microscopy with acoustic sample confinement, Nat. Commun. **10**, 669 (2019).

[36] J. Greenhall, F. Guevara Vasquez, and B. Raeymaekers, Continuous and unconstrained manipulation of microparticles using phase-control of bulk acoustic waves, Appl. Phys. Lett. **103**, 074103 (2013).

[37] T. Kozuka, K. Yasui, T. Tuziuti, A. Towata, and Y. Iida, Noncontact acoustic manipulation in air, Jpn. J. Appl. Phys. **46**, 4948 (2007).

[38] J. Greenhall, F. Guevara Vasquez, and B. Raeymaekers, Ultrasound directed self-assembly of user-specified patterns of nanoparticles dispersed in a fluid medium, Appl. Phys. Lett. **108**, 103103 (2016).

[39] C. R. P. Courtney, C.-K. Ong, B. W. Drinkwater, A. L. Bernassau, P. D. Wilcox, and D. R. S. Cumming, Manipulation of particles in two dimensions using phase controllable ultrasonic standing waves, Proc. R. Soc. A **468**, 337 (2011).

[40] A. L. Bernassau, C. R. P. Courtney, J. Beeley, B. W. Drinkwater, and D. R. S. Cumming, Interactive manipulation of microparticles in an octagonal sonotweezer, Appl. Phys. Lett. **102**, 164101 (2013).

[41] A. Grinenko, P. D. Wilcox, C. R. P. Courtney, and B. W. Drinkwater, Proof of principle study of ultrasonic particle manipulation by a circular array device, Proc. R. Soc. A **468**, 3571 (2012).

[42] C. R. P. Courtney, C. E. M. Demore, H. Wu, A. Grinenko, P. D. Wilcox, S. Cochran, and B. W. Drinkwater, Independent trapping and manipulation of microparticles using dexterous acoustic tweezers, Appl. Phys. Lett. **104**, 154103 (2014).

[43] M. Prisbrey, J. Greenhall, F. Guevara Vasquez, and B. Raeymaekers, Ultrasound directed self-assembly of three-dimensional user-specified patterns of particles in a fluid medium, J. Appl. Phys. **121**, 014302 (2017).

[44] M. Prisbrey and B. Raeymaekers, Ultrasound Noncontact Particle Manipulation of Three-dimensional Dynamic User-specified Patterns of Particles in Air, Phys. Rev. Appl. **10**, 034066 (2018).

[45] A. Marzo, S. A. Seah, B. W. Drinkwater, D. R. Sahoo, B. Long, and S. Subramanian, Holographic acoustic elements for manipulation of levitated objects, Nat. Commun. **6**, 8661 (2015).

[46] T. Schwarz, G. Petit-Pierre, and J. Dual, Viscous torque on spherical micro particles in two orthogonal acoustic standing wave fields, J. Acoust. Soc. Am. **133**, 1260 (2013).

[47] M. Scholz, B. W. Drinkwater, T. M. Llewellyn-Jones, and R. S. Trask, Counterpropagating wave acoustic particle manipulation device for the effective manufacture of composite materials, IEEE T. Ultrason. Ferr. **62**, 1845 (2015).

[48] M. Prisbrey and B. Raeymaekers, Aligning High-Aspect-Ratio Particles in User-Specified Orientations with Ultrasound-Directed Self-Assembly, Phys. Rev. Appl. **12**, 014014 (2019).

[49] J. D. N. Cheeke, *Fundamentals and Applications of Ultrasonic Waves* (CRC Press LLC, Boca Raton, 2002).

[50] H. Bruus, Acoustofluidics 7: The acoustic radiation force on small particles, Lab Chip **12**, 1014 (2012).

[51] See the Supplemental Material at http://link.aps.org/supplemental/10.1103/PhysRevApplied.14.024026 for information on the optimization algorithm and an animation demonstrating the steps to experimentally align an ellipsoidal expanded polystyrene particle.

[52] A. Marzo, T. Corkett, and B. W. Drinkwater, Ultraino: An open phased-array system for narrowband airborne ultrasound transmission, IEEE T. Ultrason. Ferr. **65**, 102 (2017).

[53] L. Cox, A. Croxford, B. W. Drinkwater, and A. Marzo, Acoustic lock: Position and orientation trapping of non-spherical sub-wavelength particles in mid-air using a single axis acoustic levitator, Appl. Phys. Lett. **113**, 054101 (2018).

[54] D. Foresti, M. Nabavi, and D. Poulikakos, On the acoustic levitation stability behaviour of spherical and ellipsoidal particles, J. Fluid Mech. **709**, 581 (2012).